OPEN

Double Pinned Perpendicular-Magnetic-Tunnel-Junction Spin-Valve Providing Multi-level Resistance States

Jin-Young Choi[1], Hansol Jun[2], Kei Ashiba[1,3], Jong-Ung Baek[2], Tae-Hun Shim[1] & Jea-Gun Park[1,2]

A new design for high density integration greater than gigabits of perpendicular-magnetic-tunnel-junction (p-MTJ) spin-valve, called the double pinned (i.e., bottom and top pinned structures) p-MTJ spin-valve achieved a multi-level memory-cell operation exhibiting four-level resistances. Three key magnetic properties, the anisotropy exchange field (H_{ex}) of the bottom pinned structure, the coercivity (H_c) of the double free-layer, and the H_c of the top pinned structure mainly determined four-level resistances producing tunneling-magnetoresistance (TMR) ratios of 152.6%, 33.6%, and 166.5%. The three key-design concepts are: i) the bottom pinned structure with a sufficiently large H_{ex} to avoid a write-error, ii) the H_c of the double free-layer (i.e., ~0.1 kOe) much less than the H_c of the top pinned structure (i.e., ~1.0 kOe), and iii) the top pinned structure providing different electron spin directions.

Perpendicular spin-transfer-torque magnetic-random access memory (p-STT MRAM), which consists of a perpendicular magnetic tunneling junction (p-MTJ) spin-valve and a selective device, has attracted great research interest because of its possibility in various applications. Recently, in particular, the p-STT MRAM cells have been utilized as embedded memory in system-on-chip for mobile and internet-of-things applications[1–5], a stand-alone memory as a solution to the dynamic-random-access-memory (DRAM) scaling limitations below the 10-nm node[6], and spin-neuron and synaptic devices for deep learning[7–9]. The p-STT MRAM has many advantages over current memory devices, such as non-volatility, fast read/write speed (~10 ns), extremely low power consumption (<1 pJ/bit), high write endurance (>10^12), and scalability[10–15].

The researches on p-STT MRAM have been based on improving three device parameters of the p-MTJ spin-valves[11–13]: the tunneling magnetoresistance (TMR) ratio greater than 150% for ensuring a memory margin, the thermal stability ($\Delta = K_u V / k_B T$, where K_u, V, k_B, and T are the magnetic anisotropy energy, the volume of the free ferromagnetic layer, the Boltzmann constant, and the temperature, respectively) above 75 for a ten-year retention-time, and the switching current density of about 1 MA/cm² for low power consumption. Moreover, these device parameters should be available at a back end of line (BEOL) temperature > 350 °C[16,17]. The conventional double MgO based p-MTJ spin-valve consist of upper and lower synthetic anti-ferromagnetic (SyAF) [Co/Pt]$_n$ multilayer separated by a Ru spacer, a $Co_2Fe_6B_2$ magnetic pinned layer, a MgO tunneling barrier, and $Co_2Fe_6B_2$ magnetic free layers, as shown in Fig. 1a: called a single pinned p-MTJ spin-valve[18]. A single pinned p-MTJ spin-valve can generate only two resistance states: the high-resistance state (HRS) from the anti-parallel spin direction, and the low-resistance state (LRS) from the parallel spin direction between the $Co_2Fe_6B_2$ free layer and the $Co_2Fe_6B_2$ pinned layer. Thus, these two different resistance states have been used to operate only single-bit p-STT MRAM memory cells. However, the scaling down for terabit-level integration of the p-STT MRAM cells, to compete with current DRAM[19], 3-dimensional (3D) NAND flash memory, and 3-dimensional cross-point memory, would be necessary to achieve the thermal stability required for 10-year retention time[20,21] and multi-level memory-cell operation like that of current 3-D NAND flash memory[22,23]. In our research, we designed a double pinned p-STT-MTJ spin-valve exhibiting multi-level (i.e., four) resistance states. The double pinned p-STT MRAM was composed of three main ferro-magnetic component layers: the bottom pinned structure, double free-layer, and top pinned structure (see Fig. 1b). The TMR ratio was maximized by introducing a

[1]MRAM Center, Department of Electronics and Computer Engineering, Hanyang University, Seoul, 04763, Republic of Korea. [2]MRAM Center, Department of Nanoscale Semiconductor Engineering, Hanyang University, Seoul, 04763, Republic of Korea. [3]Wafer Engineering Department, SUMCO CORPORATION, 1-52 Kubara, Imari, Saga, 849-4256, Japan. Correspondence and requests for materials should be addressed to J.-G.P. (email: parkjgl@hanyang.ac.kr)
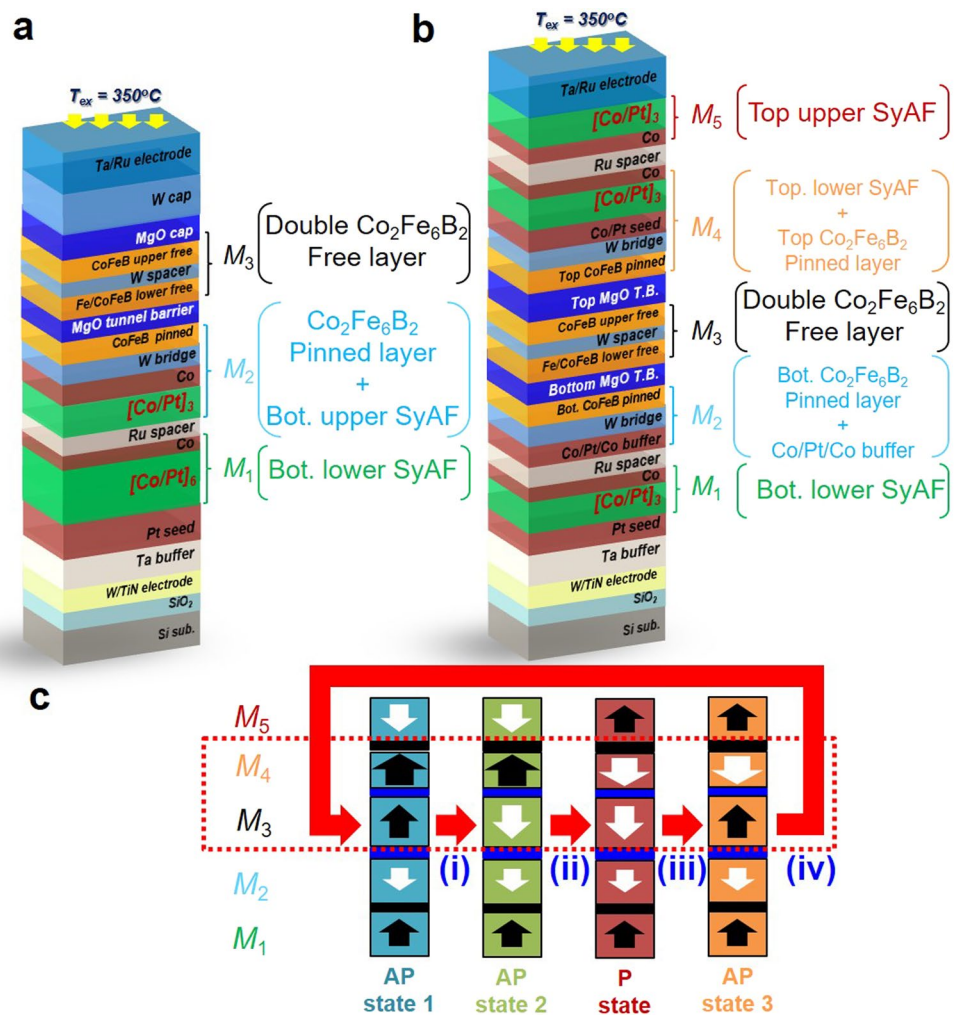
Figure 1. Schemes of p-MTJ spin-valves and design concept of the double pinned p-MTJ spin-valve. (**a**) Single pinned p-MTJ spin-valve with double free layer, (**b**) double-pinned p-MTJ spin-valve with double free layer, and (**c**) spin direction configuration of the double pinned p-MTJ spin-valve producing four-level resistance states.

bottom single SyAF $[Co/Pt]_n$ multilayers (Fig. 1b) because the upper $[Co/Pt]_3$ SyAF multilayer anti-ferro-coupled with the lower $[Co/Pt]_6$ SyAF multilayers (Fig. 1a) via a Ru spacer produced considerably high surface rough-ness[18]. The design concept of the double pinned p-STT MTJ will be explained in more detail in the following section. In addition, we investigated static magnetic properties of the double pinned p-MTJ spin-valve, tested the achievement of four-level magnetic-resistance states, and analyzed the operation mechanism of four-level resistances.

Results

Design of Double Pinned p-MTJ Spin-valve.   The double pinned p-MTJ spin-valve was vertically stacked with the bottom electrode, bottom $Co_2Fe_6B_2$ ferromagnetic pinned structure (called bottom pinned structure), double MgO based $Co_2Fe_6B_2$ ferromagnetic free layer (called the double free-layer), top $Co_2Fe_6B_2$ ferromagnetic pinned structure (called top pinned structure), and top electrode, as shown in Fig. 1b. The magnetic layers of the double pinned p-MTJ spin valve can be divided largely into five groups (M_1, M_2, M_3, M_4, and M_5 layers). The bottom electrode was made by sputtering tungsten (W) and titanium nitride (TiN) layers on a thermally oxidized 300-mm-diameter Si wafer, followed by the chemical-mechanical-planarization (CMP). For the bottom pinned structure, the Ta buffer layer was used to intersect the f.c.c. crystalline texturing of the TiN electrode since the Ta layer had an amorphous structure. The face-centered-cubic crystalline Pt-seed-layer was used to form the L10 crystalline structure of the bottom-lower SyAF [Co (0.47 nm)/Pt(0.23 nm)]$_3$ multilayer (M_1 layer) so that its spin direction was perpendicularly upward, as shown in Fig. 1c[24–26]. These layers were anti-ferro-coupled with the single Co (0.51 nm)/ Pt(0.23 nm)/Co(0.47 nm) buffer layer via Ru spacer, called the single SyAF $[Co/Pt]_n$ layer. Simultaneously, the single Co/Pt/Co buffer-layer was ferro-coupled to the bottom $Co_2Fe_6B_2$ ferromagnetic pinned layer (0.95 nm) via the W bridge layer, defined as M_2 layer. The spin direction of the M_2 layer was perpendicu-larly downward, as shown Fig. 1c. Thus, the spin directions of the M_1 and M_2 layers always face vertically inward towards each other. In particular, the anisotropy exchange field (H_{ex}) of the bottom pinned structure should be sufficiently higher than the coercivity (H_c) of the top pinned structure to fix the spin direction of both the M_1 and

M_2 layers. Then, the double $Co_2Fe_6B_2$ free-layer (M_3 layer) was stacked on the M_2 layer, where the thicknesses of the bottom MgO tunneling-barrier, Fe insertion layer, lower $Co_2Fe_6B_2$ ferromagnetic free layer, W spacer, upper $Co_2Fe_6B_2$ ferromagnetic free layer, and top MgO tunneling-barrier layer were 1.15, 0.3, 1-0.05, 0.2, 1.05, and 1.0 nm, respectively. The spin direction of M_3 layer was dependent of the polarity of the applied perpendicular-magnetic-field; i.e. vertically downward for a negative field and vertically upward for a positive field, as shown in Fig. 1c. In particular, the H_c of M_3 layer should be considerably smaller than the H_c of the top pinned structure to make four different spin direction states between the M_3 and M_4 layers [i.e., anti-parallel (AP) state 1, AP state 2, parallel (P) state, and AP state 3]. For the top pinned structure, the Fe insertion layer (0.3 nm) and top $Co_2Fe_6B_2$ ferromagnetic pinned layer (0.75 nm) were stacked on the M_3 layer. The top-lower [Co(0.47 nm)/Pt(0.23 nm)]$_3$ SyAF multilayer was ferro-coupled with the top $Co_2Fe_6B_2$ ferro-magnetic pinned-layer (0.75 nm) via a W bridge layer and Co/Pt seed layer, which is defined as M_4 layer. The spin direction of the M_4 layer was dependent of the polarity of the applied magnetic-field. Simultaneously, M_4 layer was always anti-ferro-coupled with the top-upper [Co(0.47 nm)/Pt(0.23 nm)]$_3$ SyAF multilayers (M_5 layer), via the Ru spacer. Thus, the spin direction of the M_5 layer was always in the opposite of the M_4 layers, as shown in Fig. 1(c). In particular, the number (**m**) of the top-lower [Co(0.47 nm)/Pt(0.23 nm)]$_m$ SyAF multilayers should be higher than that (**n**) of the top-upper [Co(0.47 nm)/Pt(0.23 nm)]$_n$ multilayers to produce four-different spin direction states between the M_3 and M_4 layers. If **m** is lower than **n**, only two different spin direction states would be generated between the M_3 and M_4 layers. Finally, a top Ta/Ru electrode was stacked on the M_5 layer.

In summary, the design of the double pinned p-MTJ spin-valve could produce four-different spin direction states between the M_3 and M_4 layers: AP state 1 (perpendicularly upward spin direction for both M_3 and M_4 layers), AP state 2 (spin direction facing outward between M_3 and M_4 layers), P state (downward spin direction for both M_3 and M_4 layers), and AP state 3 (spin direction facing inward between the M_3 and M_4 layers, as shown in Fig. 1c). To form four-different spin direction states, we essentially need three key-design concepts: 1) for designing the bottom pinned structure, the spin direction of the M_1 and M_2 layers should face always inward toward each other, 2) for designing M_3 layer, its H_c should be remarkably smaller than the H_c of the M_4 layer to assure to produce four-different spin direction states between the M_3 and M_4 layers, and 3) for designing the top pinned structure, the H_{ex} of the M_4 layers should be sufficiently higher than the H_c of the the M_3 layer to avoid a write-error. These three key-design concepts will be treated later in detail.

Design and Static Perpendicular-Magnetic Behaviour of Bottom Pinned Structure and Double Free-Layer.

In the bottom pinned structure (M_1 and M_2 layers) in Fig. 1b, the spin direction of the M_2 layer should always face perpendicularly inward toward with that of the M_1 layer, as shown in Fig. 1c. Thus, this bottom pinned-structure needs as large H_{ex} of the M_2 layer as possible. In our previous studies, the spin directions of the M_1 and M_2 layers are always facing perpendicularly inward against each other when the number of the bottom-upper SyAF [Co(0.4 nm)/Pt(0.2 nm)] layer (i.e., 3) is less than that of the bottom-lower SyAF [Co(0.4 nm)/Pt(0.2 nm)] layer (i.e., 6)[27–30]. Also, we implemented the p-MTJ spin-valves with a single SyAF [Co/Pt]$_n$ layer which showed large H_{ex}, as shown in Supplementary 1[18].

Using this concept, we redesigned the bottom pinned p-MTJ spin-valve (Fig. 2a,b) with double and single SyAF [Co/Pt]$_n$ layers to match that of the double pinned p-MTJ spin-valve and investigated its magnetic properties. The arrow magnitude and direction corresponded to the relative magnetic-moment and spin direction of the magnetic layers when the applied magnetic field is changed from +6.5 kOe to −6.5 kOe, as shown in Fig. 2c,d. The inset of Fig. 2c,d shows the magnetic properties of the $Co_2Fe_6B_2$ free layers (M_3 layers) of the p-MTJ spin-valve with double and single SyAF [Co/Pt]$_n$ layers. The spin direction of both structures are aligned along the external field direction when external field is high in the upward direction ($H > +5$ kOe). When the external field becomes smaller than $+1.5$ kOe, the spin direction of the M_2 layers are switched opposite the external field as the field is not strong enough to overcome the anti-ferro coupling between M_1 and M_2 layers. The M_2 layer squareness of the bottom p-MTJ spin-valve with single SyAF [Co/Pt]$_n$ layers (red box of Fig. 2d) is degraded compared to that of the spin-valve with double SyAF [Co/Pt]$_n$ layers (blue box of Fig. 2c). However, the H_{ex} is increased from 2.35 kOe to 3.44 kOe which would mean that the M_1 and M_2 layers of the p-MTJ spin-valve with single SyAF [Co/Pt]$_n$ layers is more unsusceptible to switching. In addition, the peak-to-valley (Δ_{P-V}) of the MgO tunneling barrier decreased from 2.03 nm to 1.75 nm when the thickness of the SyAF layers is reduced from 8.87 to 4.65 nm as shown in Supplementary 2. Note that the TMR ratio of the double pinned p-MTJ spin-valve is expected to increase by reducing the roughness of the MgO tunneling barrier[27–38]. Thus, the magnetic property of the double free-layer was not degraded; i.e., a good squareness and the magnetic moment of ~ 0.2 memu, as shown in the inset of Fig. 2d. This result indicates that a single SyAF [Co/Pt]$_3$ multi-layers would be very suitable as a bottom pinned structure (M_1 and M_2 layers in Fig. 1b), since it could provide a sufficiently high H_{ex} of 3.44 kOe and would increase the TMR ratio because of a lower surface roughness of the MgO tunneling-barrier. The spin direction schematic in Fig. 2c,d represents the change only when the magnetic field is changed from +6.5k Oe to −6.5 kOe. A detailed magnetic switching behavior of the p-MTJ spin-valve with double and single SyAF [Co/Pt]$_n$ layer under an external magnetic field sweep from −6.5 kOe to +6.5 kOe is shown in see Supplementary 3.

Design and Static Perpendicular-Magnetic Behaviour of Top $Co_2Fe_6B_2$ Ferro-Magnetic Pinned Structure.

In the top pinned structure, the top $Co_2Fe_6B_2$ magnetic pinned-layer was ferro-coupled with the top-lower SyAF [Co/Pt]$_m$ layer via W bridge layer (M_4 layer), which was then anti-ferro-coupled with the top-upper SyAF [Co/Pt]$_n$ layer (M_5 layer) via Ru spacer, as shown in Fig. 3a. In addition, the number of the top-lower [Co(0.47 nm)/Pt(0.23 nm)] layers **(m)** of the M_4 layer should be less than the number of the top-upper [Co(0.47 nm)/Pt(0.23 nm)] layers **(n)** of the M_5 layer, and the H_{ex} of the top pinned structure should be as large as possible to avoid a write-error. Unlike the bottom pinned structure in Fig. 2d, the top pinned structure should be able to generate four different electron-spin states between the M_3 and M_4 layer, resulting in four different
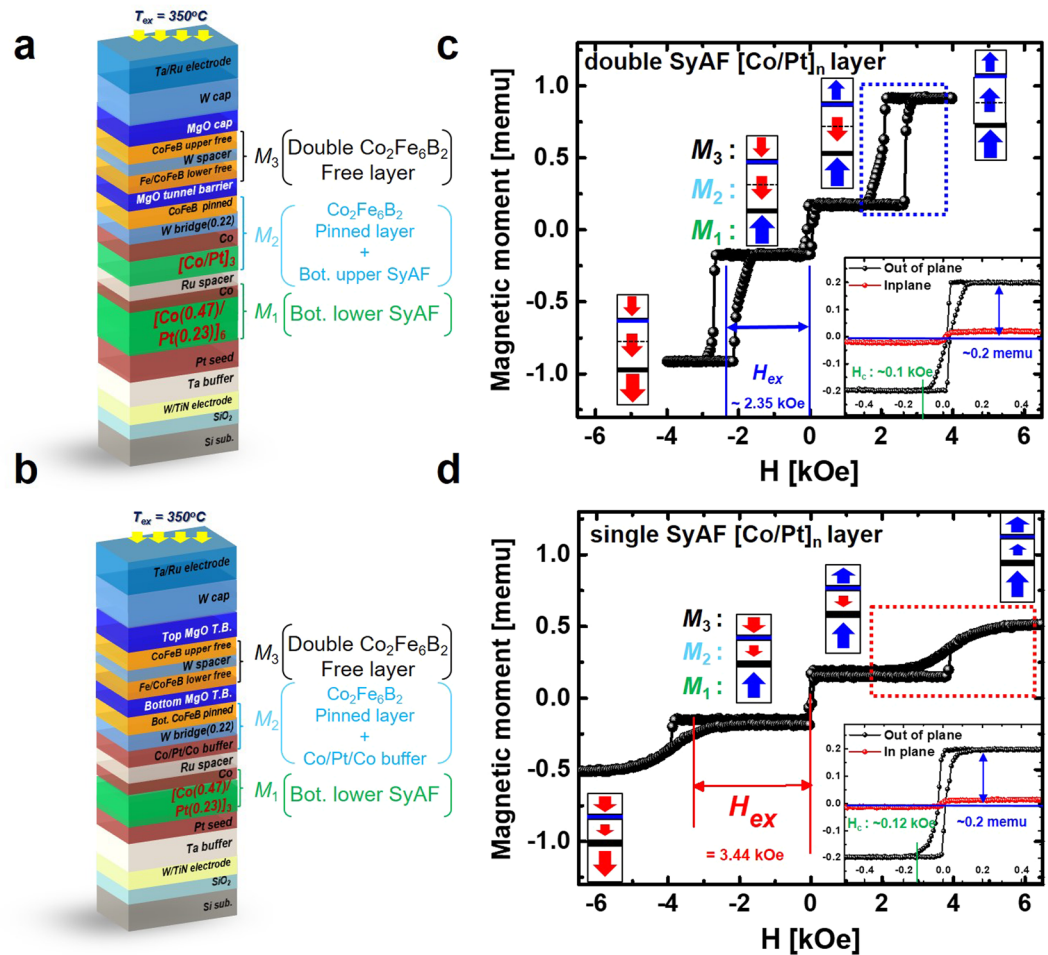
Figure 2. Dependence of static magnetic behavior (magnetic moments-vs.-applied magnetic field) of bottom pinned structure. Schemes of p-MTJ spin-valves with (**a**) double SyAF [Co/Pt]$_n$ layer and (**b**) single SyAF [Co/Pt]$_n$ layer. *M-H* curve of (**c**) double SyAF [Co/Pt]$_n$ layer (**d**) a single SyAF [Co/Pt]$_n$ layer.

resistance states. Thus, within the scanning magnetic-field range less than the H_{ex} of the top pinned structure, the spin direction of the M_4 layer could be rotated from upward to downward or downward to upward when the polarity of the magnetic-field changes from positive to negative or from negative to positive. To test whether or not the spin directions of the top pinned structure were variable, we investigated the *M-H loop* of a basic top pinned-structure with the **m:n** ratio of 6:3 of the number of [Co(0.47 nm)/Pt(0.23 nm)] multilayers in the M_4 and M_5 layers, as shown in Fig. 3b. At the applied magnetic-field of +15 kOe, the spin direction of both the M_4 and M_5 layers faced perpendicularly upward. As the magnetic-field decreased from +15 to +4 kOe, the magnetic moment decreased from +0.6 to +0.3 memu, corresponding to the magnetic moment of the M_5 layer (i.e., 0.3 memu) rotating the spin direction of the M_5 layer from upward to downward. This occurred at the H_{ex} of ~4.9 kOe arising from the anti-ferro coupling across the Ru spacer layer. As the magnetic-field decreased from +4 to −4 kOe, the magnetic moment changed from +0.3 to −0.3 memu, responding to the magnetic moment of the M_4 and M_5 layers (i.e., 0.6 memu), rotating the spin direction of the M_4 layer from upward to downward. Simultaneously, the spin direction of the M_5 layers rotated from downward to upward to hold the anti-ferro coupling via the Ru spacer stably. As a result, the spin directions of the M_4 and M_5 layers facing perpendicularly inward changed to facing perpendicularly outward. As the magnetic-field increased over −4 kOe, the spin direction of the M_5 layer rotated from upward to downward so that the spin directions of both the M_4 and M_5 layers were perpendicularly downward. In contrast, as the magnetic-field changed from negative to positive direction, the change of the spin directions of the M_4 and M_5 layers followed the same order as the magnetic-field changed from positive to negative direction. In particular, the spin directions of the M_4 and M_5 layers facing perpendicularly outward changed to facing perpendicularly inward. Thus, this top pinned structure could produce two spin directions between the M_4 and M_5 layers when the magnetic-field is greater than the H_c of the top pinned structure; facing perpendicularly outward for the negative magnetic-field and facing perpendicularly inward for the positive magnetic-field. Although the top-lower SyAF [Co(0.47 nm)/Pt(0.23 nm)]$_6$ layer and top-upper SyAF [Co(0.47 nm)/Pt(0.23 nm)]$_3$ layer and could provide variable spin directions between the M_4 and M_5 layers, the top-lower SyAF [Co(0.47 nm)/ Pt(0.23 nm)]$_6$ layer is too thick to maximize the TMR ratio of the p-MTJ spin-valve. The TMR ratio is strongly dependent on the coherent tunneling of the Δ_1 Bloch state induced from the hybridization of the Fe-$d_z{}^2$ and O-p_z orbitals at the MgO/CoFeB interface. Even a small defect at the interface reduces the coherent tunneling of the
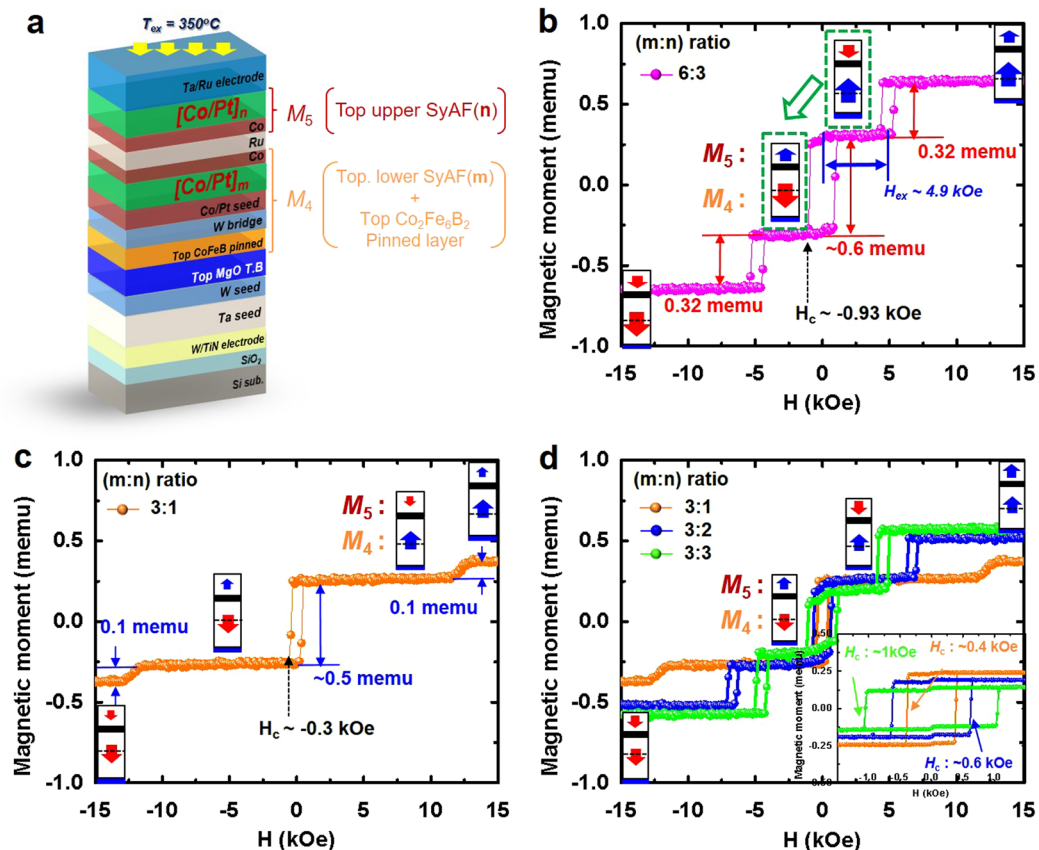
Figure 3. Dependence of static magnetic behaviour (magnetic moments-vs.-applied magnetic-field) of top pinned structure. (**a**) Scheme of top pinned structure design with [**m**] number of lower [Co/Pt] layers and [**n**] number of upper [Co/Pt] layers, (**b**) *M-H* loop of top structure with **m:n** ratio of 6:3, (**c**) *M-H* loop of top pinned structure with **m:n** ratio of 3:1, and (**d**) *M-H* loops of top pinned structures with **m:n** ratios of 3:1. 3:2, and 3:3.

spin-polarized electrons[31,39]. The roughness increases with the number of top-lower SyAF [Co/Pt]$_n$ layers from about 150 pm to 240 pm as seen in Supplementary 4. The roughness needs to be reduced to maximize the TMR ratio to assure four levels of the double pinned p-MTJ spin-valve.

To reduce the thickness of the top pinned structure, first of all, we investigated the *M-H loop* of the top pinned structure with the ratio of the [Co(0.47 nm)/Pt(0.23 nm)]$_3$ layers of the M_4 and M_5 layers (**m:n** ratio) of 3:1, as shown in Fig. 3c. Its static magnetic behaviour was similar to the top pinned structure with the ratio of **m:n** ratio of 6:3, showing the magnetic moment of the M_4 and M_5 layers, H_c, and H_{ex} were 0.1 and 0.5memu, ~0.3 kOe, and ~12 kOe. Although this top pinned structure could produce two variable spin directions between the M_4 and M_5 layers, the H_c of ~0.3 kOe was too small to generate four different spin direction states between the M_3 and M_4 layers in the double pinned p-MTJ spin-valve (Fig. 1c) since the H_c of the top pinned structure (i.e., ~0.3 kOe) was not sufficiently higher than the H_c of the double free-layer (Fig. 2d; i.e., ~0.2 kOe) to avoid the write error. Thus, we observed the dependency of the H_c of the top pinned structure on the **m:n** ratio, as shown in Fig. 3d. The **m:n** ratios of 1:3, 2:3, and 3:3 showed H_c values of ~0.4, ~0.6, and ~1 kOe, as shown in the inset of Fig. 3d, and all **m:n** ratios demonstrated two variable spin directions between the M_4 and M_5 layers. This result indicates that the H_c of the top pinned structure increases with the number of [Co(0.47 nm)/Pt(0.23 nm)]$_3$ layers in the M_5 layer, while H_{ex} decreases with the number of [Co(0.47 nm)/Pt(0.23 nm)]$_3$ layers in the M_5 layer. In particular, the **m:n** ratio of 3:3 showed a sufficient H_c (i.e., ~1 kOe), which could produce four different spin direction states between the M_3 and M_4 layers (Fig. 1c) since it is considerably larger than the H_c of the double free-layer (~0.1 kOe) (Fig. 2d). Recall that at the **m:n** ratio of 3:3 the static magnetic moment of the M_4 layer was slightly larger than that of the M_5 layer so that the spin direction of the top pinned structure (M_4 and M_5 layers) faced vertically outward for the negative applied magnetic-field and vertically inward for the positive applied magnetic-field. If **n** is larger than **m**, the spin directions of the M_4 and M_5 layers could not be variable. Therefore, the design of choosing a proper H_c and H_{ex} of the top pinned structure would be a key research to stably produce four different spin direction states between M_3 and M_4 layers.

Static Perpendicular-Magnetic Behaviour and Multi-level TMR ratio for Double Pinned p-MTJ Spin-Valve. By combining the top (3:3 of **m:n** in Fig. 3d) and bottom p-MTJ structures with the double free-layer (Fig. 2d), we fabricated the double pinned p-MTJ spin-valve shown in Fig. 1b. The *M-H* loop of the double pinned p-MTJ spin-valve showed the H_{ex} of 4.9 kOe when the applied magnetic-field was scanned from
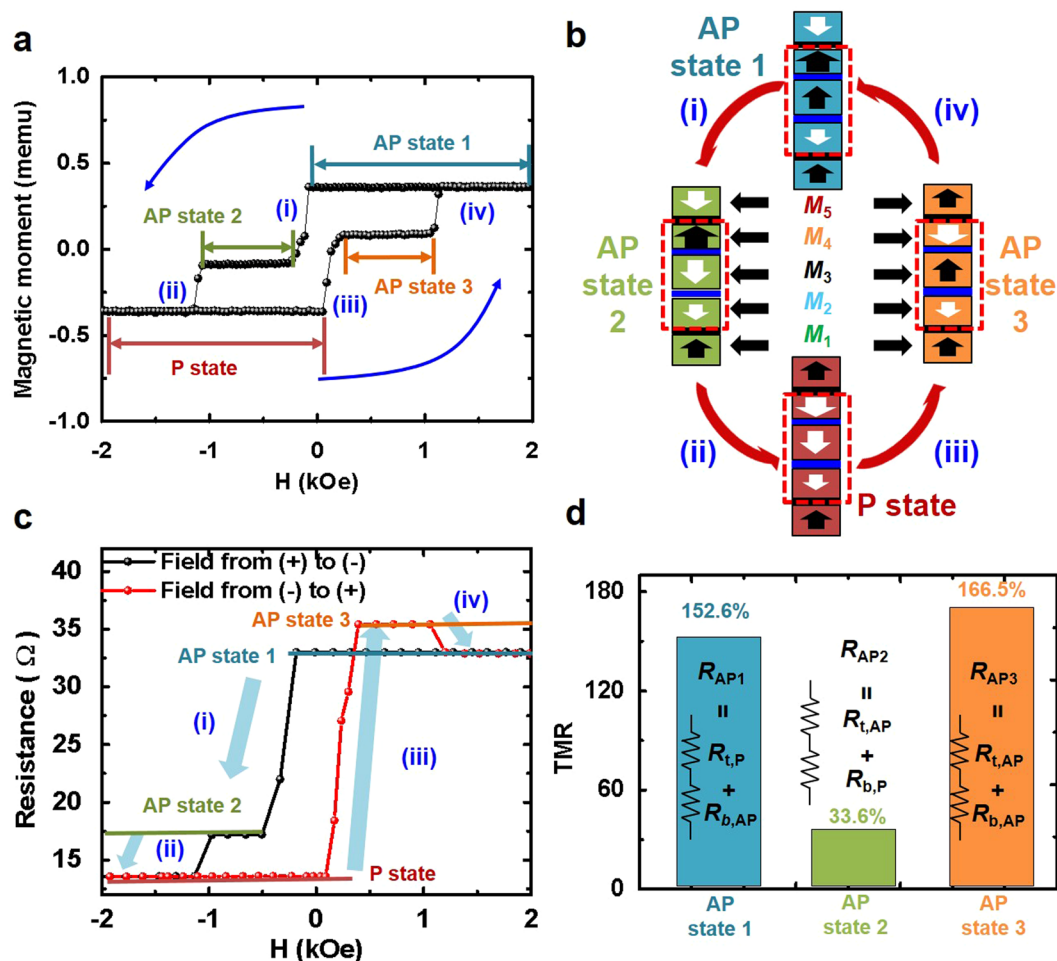
Figure 4. Magnetic and resistance properties of double pinned p-MTJ spin-valve in narrow scanning magnetic-field range (−2 kOe to +2 kOe). (**a**) *M-H* loop, (**b**) four-different spin-electron-directions depending on the polarity and magnitude of the scanning magnetic-field, (**c**) *R-H* loop of double pinned p-MTJ spin-valve with cell size of 2 μm², and (**d**) TMR ratios of double pinned p-MTJ spin-valve.

−6.5 kOe to +6.5 kOe, as shown in Supplementary 5a. In addition, the resistance-vs.-magnetic-field (*R-H*) loop presented only three resistance states, when the applied magnetic-field was scanned from $-H_{ex}$ to $+H_{ex}$ kOe, as shown in Supplementary 5b,c. In order to produce four different resistance states, thus, the maximum scanning range of the applied magnetic-field should be sufficiently less than $\pm H_{ex}$ (i.e., ~4.2 kOe) of the bottom pinned p-MTJ spin-valve, but greater than $\pm H_{ex}$ (i.e., ~1 kOe) of the top pinned structure (M_4 and M_5 layers); i.e., ±2 kOe. Thus, four different spin directions between the M_3 and M_4 layers could be stably produced when the applied magnetic-field was scanned from −2 kOe to +2kOe, as shown in the *M-H* loop of Fig. 4a. First, the AP state 1 was produced when the applied magnetic-field was scanned from +2 kOe to +0.5 kOe, where the spin directions of both the M_3 and M_4 layers were vertically upward and parallel while the spin directions of the M_4 and M_5 layers faced vertically inward toward each other via an anti-ferro-coupling, as shown Fig. 4a,b. Recall that this result corresponds to the combination of the top pinned structure (M_4 and M_5 layers) in Fig. 3d and the bottom pinned structure (M_1 and M_2 layers) with the double free-layer (M_3 layer) in Fig. 2d at the positive applied magnetic-field. Then, when the applied magnetic-field was scanned from +0.5 kOe to −0.5 kOe, the spin direction of only the M_3 layer was rotated from upward to downward while the spin directions of both the M_4 and M_5 layer did not change, generating the AP state 2, where the spin direction of the M_3 layer faced vertically outward against that of the M_4 layer, as shown in **i** in Fig. 4a,b. Furthermore, when the applied magnetic-field was scanned from −0.5 kOe to −2.0 kOe, the spin directions between the M_4 and M_5 layers facing vertically inward were rotated to face vertically outward while the spin direction of the double free-layer was sustained downward, forming the P state, where the spin directions of both M_3 and M_4 layers were vertically downward and in parallel, as shown in **ii** in Fig. 4a,b. Subsequently, when the applied magnetic-field was scanned from −2.0 kOe to +0.5 kOe, the spin direction of only the M_3 layer rotated from downward to upward while the spin directions of both the M_4 and M_5 layers remained facing vertically outward from each other, generating the AP state 3, where the spin direction of M_3 layer faced vertically inward against that of the M_4 layer, as shown in **iii** in Fig. 4a,b. Finally, the spin directions between the M_4 and M_5 layers facing vertically outward were rotated to face vertically inward while the spin direction of the M_3 layer remained facing upward, returning to the AP 1 state, where the spin directions of both the M_3 and M_4 layers facing vertically inward transited to facing vertically and parallel upward, as shown in

iv in Fig. 4a,b. As a result, four different spin directions between the M_3 and M_4 layers could be stably produced in a magnetic-field scanning range of ±2.0 kOe.

The *R-H* loop corresponding to the *M-H* loop in Fig. 4a was shown in Fig. 4c. The resistance changed from the AP state 1, AP state 2, AP state 3, P state, and AP state 1 when the applied magnetic-field was scanned from +2.0 kOe, −2.0 kOe, and +2.0 kOe. The sequence of a higher resistance of the double pinned p-MTJ spin-valve was followed by AP state 3, AP state 1, AP state 2, and P state. The highest resistance was achieved when the M_3 layers became the anti-parallel states against both the M_2 and M_4 layers; i.e., the AP state 3, corresponding to the sum of serial connection (R_{AP3}) of the anti-parallel resistance between the M_3 and M_4 layers ($R_{t,AP}$) with the anti-parallel resistance between the M_2 and M_3 layers ($R_{b,AP}$), as shown in Fig. 4d. The second highest resistance was obtained, when the M_3 layers became the parallel state against the M_4 layers while it was in the anti-parallel state against the M_2 layers; i.e., the AP state 1, responding to the sum of serial connection (R_{AP1}) of the parallel resistance between the M_3 and M_4 layers ($R_{t,P}$) with the anti-parallel resistance between the M_2 and M_3 layers ($R_{b,AP}$). The third highest resistance was achieved, when the M_3 layers became the anti-parallel state against the M_4 layers while it did the parallel state against the M_2 layers; i.e., the AP state 2, indicating to the sum of serial connection (R_{AP2}) of the anti-parallel resistance between the M_3 and M_4 layers ($R_{t,AP}$) with the parallel resistance between the M_2 and M_3 layers ($R_{b,P}$). Note that the anti-parallel resistance between the M_2 and M_3 layers ($R_{b,AP}$) is much larger than the anti-parallel resistance between the M_3 and M_4 layers ($R_{t,AP}$) since the thickness of the bottom MgO tunneling barrier (1.15 nm) was greater than that of the top MgO tunneling barrier (1.0 nm). This is confirmed by the high-resolution transmission-electro-microscopy (HR-TEM) observation shown in Supplementary 3. Thus, the resistance of the AP state 1 was larger than that of the AP state 2.

Multi-level TMR ratios of the double pinned p-MTJ spin-valve were measure by CIPT (current-in-plane tunneling) measurement scanning the magnetic-field of ±2 kOe. The TMR ratios were 152.6% for AP state 1, 33.6% for AP state 2, and 166.5% for AP state 3. These values correlated well with the four different resistance levels in the *R-H* loop in Fig. 4c. A higher TMR ratio was accounted for when the spin direction of the M_3 layer becomes anti-parallel to that of the M_2 layer (i.e., $R_{b,AP}$). This result evidently indicates that the double pinned p-MTJ-spin-valve can perform multi-level (i.e., four-level) non-volatile memory-cell operation.

Discussion

Our proposed double pinned p-MTJ spin-valve well demonstrated four-level resistance as a multi-level p-STT MRAM-cell, resulting in the TMR ratios of 152.6, 33.6, and 166.5%. The maximum TMR ratio of the double pinned p-MTJ spin-valve (166.5%) was slightly less than that of a single pinned p-MTJ spin-valve (i.e., 180%), since the Pt atoms in the top pinned structure diffused into both top and bottom MgO tunneling barrier so that the coherent tunneling of the spin-electron would be decreased as shown Supplementary 6. Thus, research on how to avoid the Pt diffusion from the top pinned structure is necessary; i.e., research on the design of a nano-scale buffer layer preventing Pt atom diffusion. In addition, to minimize a write-error originated between four-level resistances, the differences between four-level resistances should be as constant as possible. Thus, research on choosing a proper thickness between the top and bottom MgO tunneling barriers is also necessary. Success in the above-mentioned research will enable us to fabricate a terabit-level p-STT MRAM for embedded, stand-alone, and neuromorphic devices.

Methods

The p-MTJ spin-valves were fabricated using a 12-inch-wafer multi-chamber cluster-magnetron sputtering-system under a high vacuum (less than 1×10^{-8} torr). In particular, the conventional p-MTJ spin-valve with the top double free-layer and double SyAF $[Co/Pt]_n$ layers in Fig. 1a were fabricated by vertically stacking a 12-inch SiO_2 wafer, W/TiN bottom electrode, Ta buffer layer, Pt seed layer, bottom-lower SyAF [Co(0.47 nm)/ Pt(0.23 nm)]$_6$ layers/Co(0.51 nm) (M_1 layer), Ru spacer layer (0.85 nm), Co(0.51 nm)/Pt(0.23 nm)/ bottom-upper SyAF [Co(0.47 nm)/Pt(0.23 nm)]$_3$ layers, and a Co buffer layer (0.47 nm). The W bridge layer of 0.22 nm was used to ferro-couple the bottom-upper SyAF layer to the pinned layer. The p-MTJ consisted of a $Co_2Fe_6B_2$ bottom pinned layer (1.05 nm), MgO tunneling barrier (1.15 nm), Fe insertion layer (0.3 nm), $Co_2Fe_6B_2$ free layers (1.05 nm), W spacer layer (0.4 nm), $Co_2Fe_6B_2$ (1.05 nm), and MgO (1.0 nm)/W capping layer. The ferro-coupled bottom-upper SyAF [Co(0.47 nm)/Pt(0.23 nm)]$_3$ layers and the $Co_2Fe_6B_2$ bottom pinned layer is defined as the M_2 layer. The bottom pinned structure of the double pinned p-MTJ spin-valve using a single SyAF $[Co/Pt]_n$ layer and double free-layer were fabricated wherein the ratio of the number of $[Co/Pt]_n$ layers between the upper and lower SyAF $[Co/Pt]_n$ layer was varied from 3:6 (i.e., a double SyAF $[Co/Pt]_n$ layer) to 0:3, as shown in Fig. 1b. In addition, a Co/Pt/Co buffer layer was used to bridge instead of the top-upper SyAF [Co(0.47 nm)/Pt(0.23 nm)]$_3$ layer (compare Fig. 1a,b). The MgO capping layer of the conventional double MgO-based p-MTJ spin-valve structure was used as the top MgO tunneling barrier followed by an Fe insertion layer (0.3 nm), $Co_2Fe_6B_2$ (0.75 nm) top pinned layer, W bridge layer (0.42 nm), Co(0.47 nm)/Pt(2 nm) buffer layer, and top-lower SyAF [Co(0.47 nm)/ Pt(0.23 nm)]$_3$ layer/ Co(0.51 nm). The ferro-coupled $Co_2Fe_6B_2$ top pinned layer and the top-lower SyAF [Co(0.47 nm)/Pt(0.23 nm)]$_3$ layer is defined as the top-pinned layer (M_4 layer). Following the M_4 layer is the Ru spacer layer (0.85 nm), Co(0.51 nm)/Pt(0.23 nm)/top-upper SyAF [Co(0.47 nm)/Pt(0.23 nm)]$_3$ layer (M_5 layer), and Ta/Ru top electrode. The spin-valves were *ex-situ* annealed at 350 °C for 30 min under a vacuum below 10^{-6} torr and a perpendicular magnetic-field of 3 tesla. The TMR ratios of the double pinned p-MTJ spin-valves fabricated on 12-inch Si wafers were estimated by using CIPT at room temperature. The wafers were cut into $1 \times 1 \, cm^2$ pieces. The magnetic properties of the double pinned spin-valves were characterized by using vibrating-sample magnetometer (VSM) at room temperature. The *R-H* curve was measured with a p-MTJ spin-valve with the cell size of 2-μm × 2-μm. The 2-μm-scale p-MTJ spin-valves were wire-bonded to the sample holder and were installed into a home-made electrical probing system with a ~1 Tesla electromagnet using a Keithley 236 source measure unit and Agilent B2902A semiconductor parameter analyzer.

References

1. Song, Y. J. *et al*. Highly Functional and Reliable 8Mb STT-MRAM Embedded in 28nm Logic. *IEDM*, 27.2.1–27.2.4, https://doi.org/10.1109/IEDM.2016.7838491 (2017).
2. Antonyan, A., Pyo, S., Jung, H. & Song, T. Embedded MRAM Macro for eFlash Replacement. *IEEE International Symposium on Circuits and Systems* (ISCAS), 2–5, https://doi.org/10.1109/ISCAS.2018.8351201 (2018).
3. Jan, G. *et al*. Demonstration of fully functional perpendicular STT-MRAM chips with sub-5ns writing for non-volatile embedded memories. *Dig. Tech. Pap. - Symp. VLSI Technol.* 093008, 8–9, https://doi.org/10.1109/VLSIT.2014.6894357 (2014).
4. Lu, Y. *et al*. Fully functional perpendicular STT-MRAM macro embedded in 40 nm logic for energy-efficient IOT applications. *IEEE Int. Electron Devices Meeting, IEDM*, 26.1.1–26.1.4, https://doi.org/10.1109/IEDM.2015.7409770 (2016).
5. Aitken, R. *et al*. Device and technology implications of the Internet of Things. *Symp. VLSI Technol. Dig. Tech. Papers*, 1–4, https://doi.org/10.1109/VLSIT.2014.6894339 (2014).
6. Durlam, M. *et al*. MRAM Memory for Embedded and Stand Alone Systems, *IEEE Int. Conf. Integr. Circuit Des. Technol.* (ICICDT), 75–78, https://doi.org/10.1109/ICICDT.2007.4299546 (2007).
7. Grollier, J., Querlioz, D. & Stiles, M. D. Spintronic Nanodevices for Bioinspired Computing. *Proc IEEE Inst Elestr Electron Eng.* **104**(10), 2024–2039, https://doi.org/10.1109/JPROC.2016.2597152 (2016).
8. Vincent, A. F. *et al*. Spin-Transfer Torque Magnetic Memory as a Stochastic Memristive Synapse for Neuromorphic Systems. *IEEE Transactions on Biomedical Circuits and Systems* **9**(2), 166–174, https://doi.org/10.1109/TBCAS.2015.2414423 (2015).
9. Sengupta, A., Choday, S. H., Kim, Y. & Roy, K. Spin orbit torque based electronic neuron. *Appl Phys. Lett.* **106**, 143701, https://doi.org/10.1063/1.4917011 (2015).
10. Ikeda, S. *et al*. A perpendicular-anisotropy CoFeB–MgO magnetic tunnel junction. *Nature Materials* **9**, 721–724 (2010).
11. Tillie, L. B. *et al*. P-STT-MRAM Thermal stability and modeling of its temperature dependence. *Int. Symp. VLSI Technol. Syst. Appl.* 1–2, https://doi.org/10.1109/VLSI-TSA.2018.8403857 (2018).
12. Yakata, S. *et al*. Influence of perpendicular magnetic anisotropy on spin-transfer switching current in CoFeB/MgO/CoFeB magnetic tunnel junctions. *J. Appl. Phys.* **105**, 07D131, https://doi.org/10.1063/1.3057974 (2009).
13. Park, J. G. *et al*. Challenging issues for terra-bit-level perpendicular STT-MRAM. *IEEE Int. Electron Devices Meeting, IEDM*, 19.2.1–19.2.4, https://doi.org/10.1109/IEDM.2014.7047081 (2015).
14. Lee, D. Y., Shim, T. H. & Park, J. G. Effects of Pt capping layer on perpendicular magnet anisotropy in pseudospin valves of Ta/CoFeB/MgO/CoFeB/Pt magnetic-tunneling junctions. *Appl. Phys. Lett.* **102**, 212409, https://doi.org/10.1063/1.4808084 (2013).
15. Kent, A. D. & Worledge, D. C. A new spin on magnetic memories. *Nature Nanotechnology* **10**(3), 187–191 (2015).
16. Wen, Z. *et al*. A 4-Fold-Symmetry Hexagonal Ruthenium for Magnetic Heterostructures Exhibiting Enhanced Perpendicular Magnetic Anisotropy and Tunnel Magnetoresistance. *Adv. Mater.* **26**(37), 6483–6490, https://doi.org/10.1002/adma.201401959 (2014).
17. Honjo, H. *et al*. 10 nm ϕ perpendicular-anisotropy CoFeB-MgO magnetic tunnel junction with over 400 °C high thermal tolerance by boron diffusion control. *Symp. VLSI Technol. Dig. Tech. Papers*, 160–161, https://doi.org/10.1109/VLSIT.2015.7223661 (2015).
18. Choi, J. Y., Lee, D. G., Baek, J. U. & Park, J. G. Double MgO-based Perpendicular Magnetic-Tunnel-Junction Spin-valve Structure with a Top $Co_2Fe_6B_2$ Free Layer using a Single SyAF $[Co/Pt]_n$ Layer. *Sci. Rep.* **8**, 2139 (2018).
19. DRAM Technology/Products Roadmap. "Technology Roadmaps." TechInsights, www.techinsights.com/technology-intelligence/overview/technology-roadmaps/.
20. Peng, S. *et al*. Interfacial Perpendicular Magnetic Anisotropy in Sub-20 nm Tunnel Junctions for Large-Capacity Spin-Transfer Torque Magnetic Random-Access. *Memory, IEEE Magn. Lett.* **8**, 3105805, https://doi.org/10.1109/LMAG.2017.2693961 (2017).
21. Perrissin, N. *et al*. A highly thermally stable sub-20 nm magnetic random-access memory based on perpendicular shape anisotropy. *Nanoscale* **10**, 12187–12195, https://doi.org/10.1039/C8NR01365A (2018).
22. Jang, J. J. *et al*. Vertical Cell Array using TCAT(Terabit Cell Array Transistor) Technology for Ultra High Density NAND Flash Memory. *Symp. VLSI Technol.* 14–15 (2009).
23. Cai, Y. *et al*. Experimental Characterization, Optimization, and Recovery of Data Retention Errors in MLC NAND Flash Memory, Preprint at arXiv:1805.02819 (2018).
24. Leroux, C., Cadeville, M. C., Bohnes, V. P., Inden, G. & Hinz, F. Comparative investigation of structural and transport properties of $L1_0$ NiPt and CoPt phases; the role of magnetism. *J. Phys. F Met. Phys.* **18**, 2033–2051, http://iopscience.iop.org/0305-4608/18/9/021 (1988).
25. Park, J. H. *et al*. Co∕Pt multilayer based magnetic tunnel junctions using perpendicular magnetic anisotropy. *J. Appl. Phys.* **103**, 07A917, https://doi.org/10.1063/1.2838754 (2008).
26. Maat, S., Takano, K., Parkin, S. S. P. & Fullerton, E. E. Perpendicular Exchange Bias of Co/Pt Multilayers. *Phys. Rev. Lett.* **87**, 87202-1–87202-4 (2001).
27. Lee, D. Y., Lee, S. E., Shim, T. H. & Park, J. G. Tunneling-Magnetoresistance Ratio Comparison of MgO-Based Perpendicular-Magnetic-Tunneling-Junction Spin Valve Between Top and Bottom $Co_2Fe_6B_2$ Free Layer Structure. *Nanoscale Res. Lett.* **11**, 433, https://doi.org/10.1186/s11671-016-1637-9 (2016).
28. Takemura, Y., Lee, D. Y., Lee, S. E. & Park, J. G. Dependency of tunneling magnetoresistance ratio on Pt seed-layer thickness for double MgO perpendicular magnetic tunneling junction spin-valves with a top $Co_2Fe_6B_2$ free layer *ex-situ* annealed at 400 °C. *Nanotechnology.* **27**, 485203 (2016).
29. Lee, D. Y., Hong, S. H., Lee, S. E. & Park, J. G. Dependency of Tunneling-Magnetoresistance Ratio on Nanoscale Spacer Thickness and Material for Double MgO Based Perpendicular-Magnetic-Tunneling-Junction. *Sci. Rep.* **6**, 38125 (2016).
30. Lee, S. E., Shim, T. H. & Park, J. G. Perpendicular magnetic tunnel junction (p-MTJ) spin-valves designed with a top $Co_2Fe_6B_2$ free layer and a nanoscale-thick tungsten bridging and capping layer. *NPG Asia Materials* **8**, e324 (2016).
31. Shen, W. *et al*. Effect of film roughness in MgO-based magnetic tunnel junctions. *App. Phys. Lett.* **88**(18), 182508, https://doi.org/10.1063/1.2201547 (2006).
32. Jeon, M. S. *et al*. The dependency of tunnel magnetoresistance ratio on nanoscale thicknesses of $Co_2Fe_6B_2$ free and pinned layers for $Co_2Fe_6B_2$/MgO-based perpendicular-magnetic-tunnel-junctions. *Nanoscale* **7**(17), 8142–8148, https://doi.org/10.1039/C5NR01140J (2015).
33. Lee, D. Y., Seo, H. T. & Park, J. G. Effects of the radio-frequency sputtering power of an MgO tunneling barrier on the tunneling magneto-resistance ratio for $Co_2Fe_6B_2$/MgO-based perpendicular-magnetic tunnel junctions. *J.Mater. Chem. C* **4**, 135–141, https://doi.org/10.1039/C5TC03669K (2016).
34. Lee, S. E., Takemura, Y. & Park, J. G. Effect of double MgO tunneling barrier on thermal stability and TMR ratio for perpendicular MTJ spin-valve with tungsten layers. *App. Phys. Lett.* **109**(18), 182405, https://doi.org/10.1063/1.4967172 (2016).
35. Chae, K. S., Shim, T. H. & Park, J. G. Dependency of anti-ferro-magnetic coupling strength on Ru spacer thickness of $[Co/Pd]_n$-synthetic-anti-ferro-magnetic layer in perpendicular magnetic-tunnel-junctions fabricated on 12-inch TiN electrode wafer. *J. Appl. Phys.* **116**(3), 033904, https://doi.org/10.1063/1.4887352 (2014).
36. Chae, K. S., Lee, D. Y., Shim, T. H., Hong, J. P. & Park, J. G. Correlation of the structural properties of a Pt seed layer with the perpendicular magnetic anisotropy features of full Heusler-based Co_2FeAl/MgO/$Co_2Fe_6B_2$ junctions via a 12-inch scale Si wafer process. *Appl. Phys. Lett.* **103**, 162409, https://doi.org/10.1063/1.4824306 (2013).
37. Lee, D. Y., Shim, T. H. & Park, J. G. Effect of coupling ability between a synthetic antiferromagnetic layer and pinned layer on a bridging layer of Ta, Ti, and Pt in perpendicular-magnetic tunnel junctions. *Nanotechnology* **27**(29), 295705 (2016).

38. Lee, S. E., Shim, T. H. & Park, J. G. Co$_2$Fe$_6$B$_2$/MgO-based perpendicular spin-transfer-torque magnetic-tunnel-junction spin-valve without [Co/Pt]$_n$ lower synthetic-antiferromagnetic layer. *Nanotechnology* **26**(47), 475705 (2015).
39. Yang, H. X. *et al.* First-principles investigation of very large perpendicular magnetic anisotropy at Fe|MgO and Co|MgO interfaces. *Phys. Rev. B* **84**, 054401 (2011).

Acknowledgements

Author Contributions

J.Y. Choi and J.G. Park conceived and designed the study. J.Y. Choi, H. Jun, K. Ashiba fabricated all patterns and carried out experiments, with the help of J.G. Park. Contributions to the measurements were made by J.Y. Choi, H. Jun, K. Ashiba, and J.U. Baek. All authors contributed to discussions regarding the research. J.Y. Choi, T.H. Shim and J.G. Park wrote the manuscript.

Additional Information

Supplementary information accompanies this paper at https://doi.org/10.1038/s41598-019-48311-0.

Competing Interests: The authors declare no competing interests.

Publisher's note: Springer Nature remains neutral with regard to jurisdictional claims in published maps and institutional affiliations.